Effect of well configuration, well placement and reservoir characteristics on the performance of marine gas hydrate reservoir

Neelam Choudhary, Jyoti Phirani

Department of Chemical Engineering , Indian Institute of Technology Delhi, Hauz Khas, Delhi-110016, India

Abstract

Reservoir simulations are used to forecast the long-term gas production from gas hydrate reservoirs. In the present work, we explore different well placements and well configurations to analyze the gas production strategy for an oceanic, unconfined, class-2, gas hydrate reservoir using an in-house three-dimensional finite volume simulator. In the past, for depressurization in an unconfined class-2 reservoirs,isolation of the aquifer zone by well placement is suggested. We show that for high pressure conditions in marine gas hydrate reservoirs, depressurization is ineffective even with horizontal producer placed far away from the aquifer. Therefore, Warm water injection is necessary along with depressurization. We demonstrate that, the injector placement and configuration determines the gas production behavior and producer conditions do not significantly impact the production potential. We also find that the unconfined aquifer below the hydrate zone helps in the warm water convection and proximity of the injector to the aquifer improves gas production behaviour. However, for unconfined class-2 gas hydrate reservoirs with low initial pressure, depressurization is effective and leads to a very high recovery (80%) of the gas. The reservoir porosity governs the warm water injection which affects the available dissociation energy to the gas hydrates and hence the gas recovery. In a layered reservoir, the porosity of the hydrate layer adjacent to the overburden has significant impact on the gas production due to the available dissociation energy from the overburden.

Keywords

Gas hydrates, class-2, unconfined reservoir simulations, well arrangements.

Nomenclature

ϕ absolute porosity

ϕ^e fluid phases effective porosity

ϕ_o reference porosity

$InJP - Y$ InJP-pressure at injection well Y-value of injection pressure

Email address: jphirani@chemical.iitd.ac.in (Jyoti Phirani)

$IP - X$ IP-initial pressure of reservoir X-value of initial pressure

K absolute permeability

k permeability of the phase

k_o reference permeability

k^o_{rj} end point relative permeability

n_j phase exponential parameter

P_{ce} entry capillary pressure

S_A water saturation

S^e_{Ar} Aqueous residual saturation

S^e_{Gr} Gas residual saturation

S_G gas saturation

S^e_j saturation of mobile phase

k_r phase relative permeability

$S^{e^*}_j$ normalized saturation of the gas or aqueous phase

1. Introduction

Gas hydrates are crystalline clathrate structures composed of gas and water molecules, crystallized at low temperature and high pressure conditions. Hydrates of methane are globally present in abundance in permafrost and in oceanic deep water sediments [1]. This is because, the gas formed in deeper sediments rises and reaches water filled sediments which have favorable pressure and temperature conditions for hydrate formation [2, 3]. Large volume of methane gas, approximately $10^{18}m^3$, is stored in the methane gas hydrate reservoirs [4]. Extracting methane from hydrate reservoirs will be a significant step towards achieving energy reliability and avoiding any climatic change due to their spontaneous dissociation [5, 6]. However, the spontaneous dissociation under the seabed can vary in time scale and may vary based on the depth of the seabed [4, 7, 8, 9, 10].

Gas hydrates can be decrystallized into methane and water either by decreasing pressure or increasing temperature according to the equation;

$$CH_4.nH_2O(h) \rightleftharpoons CH_4(g) + nH_2O(w), \tag{1}$$

where, n represents the hydration number which is approximately 6 for methane hydrate. The decrystallization of the methane gas hydrates can be predicted using hydrate Pressure-Temperature equilibrium curve (P-T curve) [11] as shown in Fig.1. The phase diagram has two phase boundaries. The vertical line shows the aqueous and ice phase equilibrium curve at 273.15 K and the G-A-H

curve shows hydrate and gas equilibrium boundary. The aqueous phase is present above 273.15 K temperature, and ice is present below 273.15 K. The gas phase is stable in the region below the G-A-H equilibrium curve and the hydrate is stable in the region above the curve. All the four phases can coexist at the quadruple point.

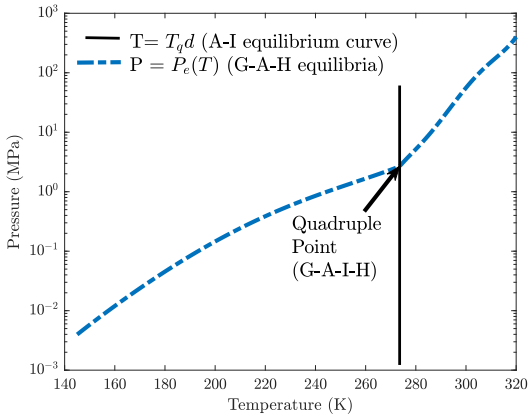

Figure 1: Pressure-Temperature equilibrium diagram for methane gas hydrates given by Sloan [11]

Based on the crystalline structure and the formation conditions of the gas hydrates, four methods and their combinations are proposed for gas production from these reservoirs: depressurization, thermal stimulation, inhibitor injection, and CO_2 injection. In the depressurization method [12, 13, 14, 15, 16, 17, 18], the pressure in the production well is decreased to reduce the reservoir pressure below the hydrate stability pressure. In thermal stimulation [18, 19, 20, 21, 22], the reservoir temperature is increased by injecting warm water or steam to dissociate the hydrates. The heating of the water is costly, therefore, water from a near-by deeper oil well or from a deeper aquifer can be sourced to reduce the cost [18, 22]. In the inhibitor injection process [23, 24, 25, 26], the chemicals such as alcohol, salt are injected along with the water to inhibit the hydrate formation. The inhibitors inhibit the hydrate formation by shifting the equilibrium pressure-temperature curve upwards. However, inhibitors are expensive, and their precipitation can block the pores [27]. In the CO_2 injection method [28, 29, 30], compressed CO_2 is injected which replaces methane molecules in hydrate crystals resulting in simultaneous CO_2 sequestration and methane production. In this case, CO_2 hydrates are formed releasing heat which can be used for methane hydrate dissociation [30]. CO_2 hydrates are formed by replacing methane molecules from the water cages [31]. In continuum, we model this as exothermic formation of CO_2 hydrate and endothermic dissociation of methane hydrates [30, 32, 33, 34]. However, this process becomes costly as high pressure CO_2 is required. Therefore, depressurization method is considered as the most efficient and economic method [35].

In Fig.2, the gas hydrate reservoirs around the world with their depth and thickness are shown. India has discovered large gas hydrate reservoirs at three sites; in Krishna-Godavari basin, Andaman Sea and Mahanadi basin. NGHP-02-09 and NGHP-02-16 sites at Krishna-Godavari basin

has the deepest methane hydrate reservoirs known so far [36]. Gas hydrate reservoirs are classified based on the underburden and overburden layers into four types: Class 1 [37]; Class 2 [38, 39, 40]; Class 3[41]; Class 4 [12]. In this work we consider Class 2 methane hydrate reservoirs found in India's Krishna-Godavari basin, where a water layer is present below the hydrate layer. Class 2 reservoirs are of two types: confined and unconfined. In confined reservoirs, the water layer below the reservoir is small, while in the unconfined reservoir the water layer is huge in comparison to the hydrate layer. The bottom aquifer layer plays an important role in hydrate dissociation using depressurization from class-2 hydrate reservoir as it provides the heat of dissociation[42]. Li et al., [42] studied class-2 confined reservoir using depressurization method and reported that the hydrate dissociation is affected by pressure drop propagation and the energy transfer from over-burden and under-burden layers of the reservoir. However, as the thickness of the aquifer layer increases, the gas production is reduced. Phirani et al.,[19] reported that depressurization method is sufficient for a class 2 confined reservoir but in an unconfined hydrate reservoir, depressurization does not provide satisfactory results because of the water inflow from the aquifer. A combination of depressurization and thermal stimulation method was proposed for unconfined reservoir where wells were placed vertically. Wang et al.,[43], Zhao et al., [44] and Wang et al., [45] also proposed warm water injection along with the depressurization method to achieve higher economic feasibility. The gas production behavior of an unconfined class-2 reservoir is under studied for well configuration and well placements.

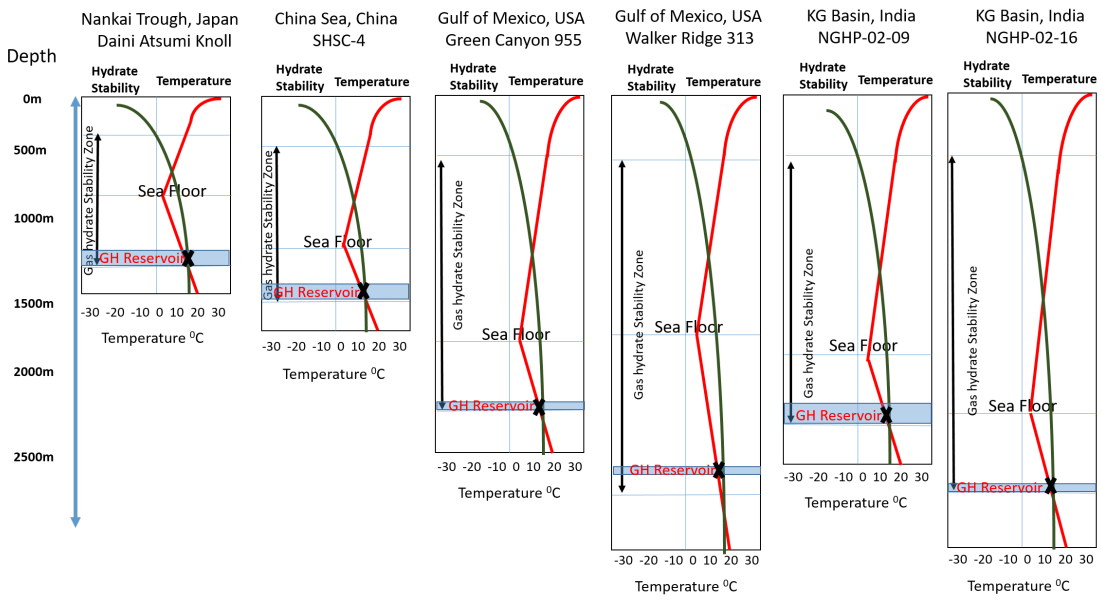

Figure 2: Details of the oceanic gas hydrate reservoirs [46]

The practicality of gas recovery from methane hydrates is evident from short term offshore field production tests which has been conducted in the past. Japan conducted a field test in 2013 and 2017 in Eastern Nankai Trough[47, 48]. In 2017, China also produced methane gas during a production test in South China Sea[49]. Depressurization method was used during these field tests.

These field tests exhibit the possibility of the methane production from the gas hydrate reservoirs, however some technical and geological issues still exist challenging the long term production [47, 48, 50]. Therefore, to understand the flow behavior inside the reservoir and to get insights about the potential problems during long term reservoir production, numerical simulations are used.

Numerical simulations provide an effective low cost prediction method [51] to analyze the gas production potential of a reservoir by studying the different well locations, well configuration, production methods, impact of different mechanical and geological conditions. Recent studies on the gas production potential of a reservoir using numerical simulations provides a better outlook on various gas production scenarios. Using reservoir simulations we now know that class-1 gas hydrate reservoirs are less challenging and promising production targets, however the free gas layer contributes more to the produced gas than the hydrate layer [52, 53, 54, 55]. Class-2 and class-3 gas hydrate deposits limit the pressure drop in the reservoir and require thermal stimulation for the production, which makes them more challenging [52, 53]. Class-3 deposits do not have a mobile free gas or water layer in contact with the hydrate layer, therefore, the hydrate dissociation is difficult for both depressurization and thermal stimulation method [52, 53]. Class-4, low saturation methane gas hydrate accumulations are not economically viable for gas production [56]. Simulations of class-2 reservoirs, inform that the depressurization alone is sufficient for confined methane gas hydrate reservoirs, however, as the porosity and the permeability of the reservoir increase, thermal stimulation is required even in confined methane gas hydrate reservoirs [18]. Simulations also helped to determine that in oceanic methane gas hydrate reservoirs, vertical wells do not produce significant methane gas using depressurization and impermeable overburden boundaries are important [1, 57]. The underburden permeability also significantly affect the gas production because of the water influx from the aquifer at the bottom. Therefore, the permeability of surrounding areas should be considered in the simulations [50]. The completion intervals are advised to be avoided in the high permeability water layer, in order to block the water inflow inside the hydrate layer and to increase the gas production while using depressurization method [12, 17, 58]. Also, in ultra deep water, as in Krishna-Godavari basin NGHP-02-16 site, less then 10 MPa pressure at bottom hole is suggested [59]. Single vertical wells are not suitable as the excessive water production is involved, however, multiple wells systems can be effective method for gas production at NGHP-02-09 site [40, 60]. Wang et al., [43] suggested the advantages of multiple well system over the single well placement by numerical simulations.

Most of the reservoir simulation studies are done on the homogeneous reservoirs, but these geological hydrate reservoirs are inherently heterogeneous because of the layering of the sediment deposited at different geological times [17, 61, 62]. The previous reservoir simulation studies suggests that in the heterogeneous reservoir, the gas recovery depends upon the depressurization potential and the total hydrate present in the reservoir but the location of hydrate dissociation may change depending on permeability of each layer, leading to the mechanical weak points at different locations [12, 17]. However, the impact of layering in an unconfined reservoir needs further exploration.

In the present work, we first explore an unconfined homogeneous class-2 methane hydrate reservoir block similar to the Krishna-Godavari basin NGHP-02-09 site, using depressurization method as well as a combination of the depressurization and warm water injection for gas production potential. The reservoir is assumed to have an impermeable overburden and the permeable underburden layer. We study the multiple well systems to increase the overall gas production where the bottom hole pressure is assumed to be 4 MPa. Multiple well placements and configurations are explored to isolate water bearing sand and to increase the effectiveness of depressurization method at NGHP-02-09 site [63]. As the horizontal well technology has been successfully used to produce methane gas from gas hydrate reservoirs in the second offshore production test in South China Sea [64], we show the effectiveness of horizontal wells and their placement for class-2 reservoirs. The production strategy is dependent on the initial condition and petrophysical characteristics of the reservoir. We examine the sensitivity of operating conditions for various reservoir characteristics to maintain the production. The geological reservoirs are inherently layered, therefore we analyze the production potential variations in these reservoir due to layering.

2. Reservoir Model

In this study we consider an unconfined reservoir block, about 300 m below the seafloor, similar to the KG basin NGHP-02-09 site. The reservoir is considered of 1200m length, 500m width and 30 m thickness as described in Fig.3. The top 18 m of the reservoir is hydrate layer. An infinite aquifer layer below the hydrate layer is considered which is 12m thick aquifer in our simulations. The initial temperature of the reservoir varies based on the geothermal gradient of $0.03^0C/m$ and the pressure varies with the depth of the reservoir according to the hydrostatic gradient. Mass transfer at the over-burden is restricted. To simulate an unconfined aquifer, the permeability of the bottom 3m of the aquifer layer is considered $1/10^{th}$ of the initial permeability. The water flow is allowed between bottom grid layer and the under-burden based on the pressure difference assuming constant pressure boundary condition at the under-burden. Heat transfer is allowed at both overburden and under-burden with a given heat transfer coefficient. The lateral boundaries are assumed to be in symmetry by assuming no communication with adjacent block. The space discretization of the reservoir domain is $25 \times 12 \times 10$ grid blocks. The initial reservoir conditions assumed in the model are given in Table.1.

2.1. Numerical methods used in the simulator

An In-house, 3-D finite-volume simulator which was developed by Sun and Mohanty[65] is used. The simulator solves thermal energy transfer, multi-phase fluid flow equations assuming equilibrium thermodynamics of the formation and dissociation of hydrate. It accounts for 3 components- water, methane, and hydrate in four phases – aqueous, gas, hydrate, and ice. The governing nonlinear partial differential equations (PDE's) are discretized into nonlinear algebraic equations in space and time domain. The spatial discretization is achieved by Finite volume method. The fully implicit scheme is obtained by approximating the time derivative using backward Euler method. Further,

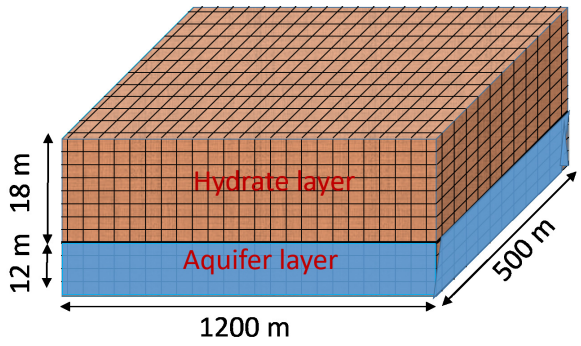

Figure 3: Reservoir description

1	Porosity (ϕ)	0.42
2	S_h in hydrate layer,	0.75
3	S_w in hydrate layer	0.25
4	S_w in aquifer layer	1
5	Permeability of hydrate layer (k_1)	0.31mD
6	Permeability of hydrate free sand (k)	1803mD
7	Initial reservoir pressure(at the bottom of the reservoir)	31.458 MPa
8	Initial reservoir temperature(at the bottom of the reservoir)	294.88 K
9	Injection pressure	50MPa
10	Injection temperature	50^0C
11	Production pressure (k_0)	4MPa

Table 1: Thermodynamic Properties

the Newton-Raphson method is used to solve the non-linear algebraic equations. The dissociation and the formation of hydrate in a grid block is assumed to be in equilibrium as the kinetics are relatively fast [66]. The phase saturation in each grid block during the hydrate dissociation process is evaluated by the primary variable switch method (PVSM) [67]. US DOE conducted a code comparison study where this simulator has been validated against several other simulators [68] and history matched with hydrate dissociation and formation experiments [69]. The governing equations are given below,

Mass balance equations

$$\frac{\partial}{\partial t}\left(\phi C^j\right) + \nabla \cdot \overline{F}^j = q^j, \tag{2}$$

Energy balance equation

$$\frac{\partial}{\partial t}\left(\phi U\right) + \nabla \cdot \overline{F}^e = -q^e, \tag{3}$$

where, ϕ stands for porosity, C^j for total mass of component for phase j (methane, water), F for flux, q for the source or sink term. U is the combined internal energy of a grid block. Flux is determined using the gas-liquid phase flow in porous media which depends on the flow properties such as absolute permeability and is described by multi-phase Darcy's law. The phase velocity is

given by

$$\overline{v_j} = -K\Big(\frac{k_{rj}}{\mu_j}\Big) \cdot \Big(\nabla P_j + \rho_j \overline{g}\Big), \tag{4}$$

where, K stands for absolute permeability, k_{rj} stands for relative permeability of the fluid phase j, μ_j for the viscosity of the fluid phase j, P_j stands for pressure of phase j, $\overline{v_j}$ for the Darcy's velocity of phase j and $\overline{g}$ for gravitational force.

2.2. ***Transport Properties considered in the model***

1	Hydrate density	$910 kg/m^3$
2	Heat conductivity of hydrate	$0.49 W/m/K$
3	Heat capacity of hydrate	$1.62 kJ/kg/K$
4	Density of ice	$917.1 kg/m^3$
5	Density of sand	$2670 kg/m^3$
6	Heat conductivity of sand	$5.57 W/m/K$
7	Heat capacity of sand	$0.83 kJ/kg/K$
8	Aqueous residual saturation	0.2
9	Gas residual saturation	0.0
10	Reference Permeability (k_0)	$100 md$
11	Reference Porosity (ϕ_0)	0.28
12	Permeability Rock Constant (β)	2
13	Relative Permeability exponent for gas (n_G)	2
14	Relative Permeability exponent for water (n_w)	4
15	Pore Structure Parameter (n_c)	5

Table 2: Thermodynamic Properties

The Power law model [70, 71, 72] has been used to described effective permeability as given by,

$$K = K_o\Big(\frac{\phi^e}{\phi_0}\Big)\Big[\frac{\phi^e(1-\phi_0)}{\phi_0(1-\phi^e)}\Big]^{2\beta} \tag{5}$$

The dynamic nature of the hydrate may change the porosity ϕ_e available for the fluid phases during the hydrate formation and dissociation process, that may affect the effective permeability of the fluid phases according to equation 5. K_o stands for the reference permeability at the reference porosity (ϕ_o), β is considered to be 2. Effective porosity for the fluid phases ϕ^e is given by

$$\phi^e = \phi(S_G + S_A), \tag{6}$$

where, ϕ represents the absolute porosity, S_G represents the gas saturation and S_A represents the aqueous saturation. The capillary pressure-saturation curve and the relative permeability curves

are used from Brooks-Corey model, [73], as given below

$$k_{rG} = k^o_{rG}(S^{e^*}_G)^{nG}, \tag{7}$$

$$k_{rA} = k^o_{rA}(S^{e^*}_A)^{nA}, \tag{8}$$

$$P_c = P_{ce}(S^{e^*}_A)^{-nc}, \tag{9}$$

where, k^o_{rj} stands for the end point relative permeability, n_j for phase j exponential parameter and P_{ce} for the entry capillary pressure. $S^{e^*}_j$ stands for normalized saturation of the fluid phase based on the effective pore volume, given as,

$$S^{e^*}_j = \frac{S^e_j - S^e_{jr}}{1 - S^e_{Gr} - S^e_{Ar}}, \tag{10}$$

where S^e_j stands for the saturation of mobile phase j. The residual saturation of aqueous phase (S^e_{Ar}) is assumed to be 0.2 and 0 for gas phase residual saturation (S^e_{Gr}). The remaining constants are tabulated in Table.2. The remaining details of the simulator can be acquired from Sun and Mohanty (2006) [65].

Case	Well type	Well location	Production method
case-1	One Horizontal	Near overburden	Depressurization
case-2	One Horizontal	Near aquifer	Depressurization
case-3	Two Vertical	In the aquifer	Thermal stimulation and depressurization
case-4	Two Vertical	In the hydrate zone	Thermal stimulation and depressurization
case-5	Two Horizontal	Near overburden	Thermal stimulation and depressurization
case-6	Two Horizontal	In the middle of hydrate zone	Thermal stimulation and depressurization
case-7	Two Horizontal	Injector near aquifer producer near overburden	Thermal stimulation and depressurization
case-8	One Horizontal, one Vertical	Horizontal injector near overburden, vertical producer in aquifer	Thermal stimulation and depressurization
case-9	One Horizontal, one vertical	Horizontal producer near overburden, Vertical injector in aquifer	Thermal stimulation and depressurization

Table 3: Well placement description in the homogeneous reservoir

3. Gas production from homogeneous unconfined reservoirs

We first investigate different well configurations and well placements to evaluate the optimum gas production strategy for an unconfined, homogeneous, class-2 reservoirs. We study nine different

cases, where horizontal and vertical wells are placed in different locations and combinations in a homogeneous reservoir block, as shown in Table.3.

3.1. ***Depressurization in the homogeneous reservoir***

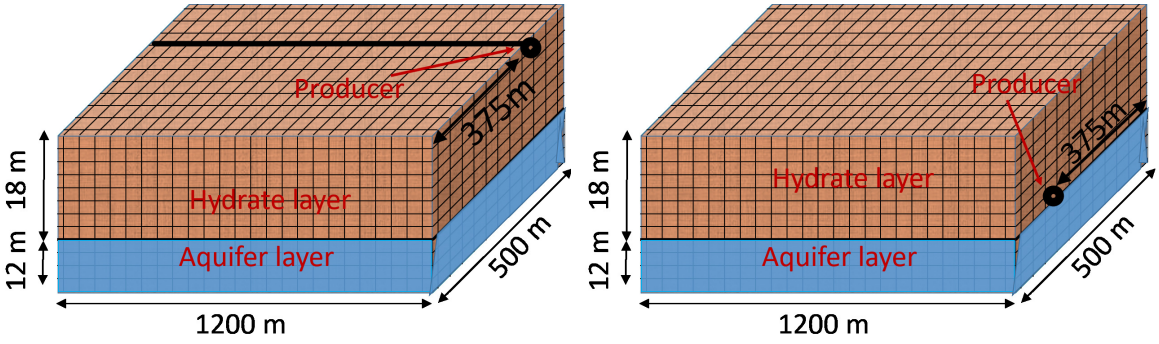

(a) Well placement for case-1 (b) Well placement for case-2

Figure 4: Well completion for case-1 and case-2 using depressurization method

In an unconfined reservoir, the pressure decrease in the reservoir is difficult because of the infinite aquifer layer below which replaces the water produced during depressurization. Phirani et al.,(2009)[19] reported that pressure drop is not effective in unconfined reservoirs when a producer is placed vertically because of the inflow of water from the unconfined aquifer below. To isolate the aquifer from the production well, we first investigate the depressurization using the wells placed horizontally in the hydrate zone. Fig.4 shows the well completion we considered in case-1 and case-2. In case-1, as shown in Fig.4a, we consider a well near the top of the reservoir to investigate isolation provided by presence of the hydrate layer. In case-2, shown in Fig.4b, we investigate a well placed near the aquifer layer for comparison. In both the cases, 4 MPa pressure is maintained at the production well for depressurization. In Fig.5a we show the cumulative gas production with time for both the cases. Only 3% of original gas in place (OGIP) is produced in both the cases as shown in Fig.5a. In case-1, the producer is placed in the low permeable hydrate bearing zone, therefore water is produced at a slow rate. However, the aquifer is able to replace the water, hence depressurization has no significant impact on the overall reservoir pressure. In case-2, the well only produces water from the aquifer attached not causing depressurization in the reservoir below the hydrate stability. The gas water ratio (GWR) in Fig.5b shows that the water production is lowest for the case-1 and very high for the case-2. This shows that even horizontal wells that can be placed away from the unconfined aquifer do not help in depressurization of the reservoir for hydrate dissociation. Therefore, warm water injection is necessary for unconfined class-2 reservoir.

3.2. ***Thermal stimulation and depressurization using vertical wells:***

For warm water injection, we first consider vertical wells, as described in Table.3. Phirani et al.,(2009)[19] considered vertical well placement in hydrate and aquifer zone. In this study we also consider wells that are placed only in the hydrate zone. We consider a 5-spot pattern and simulate

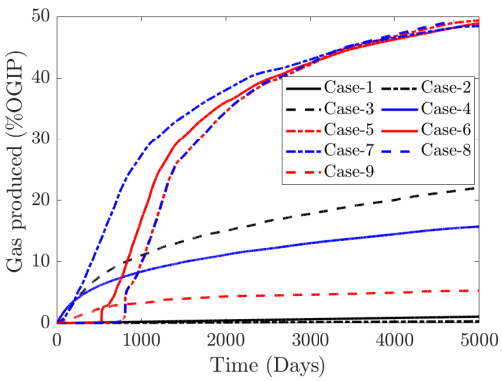

(a) Gas produced in % OGIP

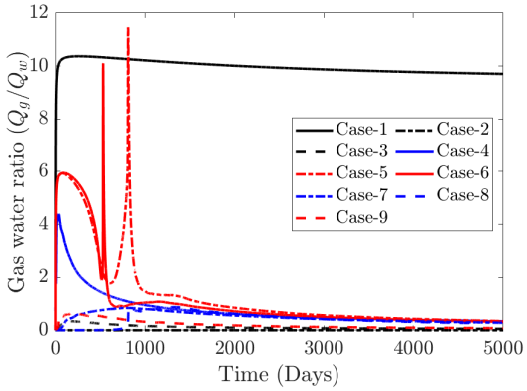

(b) Gas water ratio (GWR)

Figure 5: Gas production profiles in % OGIP and Gas-Water ratio for different cases in Table.3

quarter of 5-spot pattern with injection on one side and production from the diagonally opposite side. In case-3, wells are placed vertically in the aquifer and hydrate zone and in case-4, wells are placed vertically only in the hydrate zone. Fig.6 gives the pictorial description of case-3 and case-4.

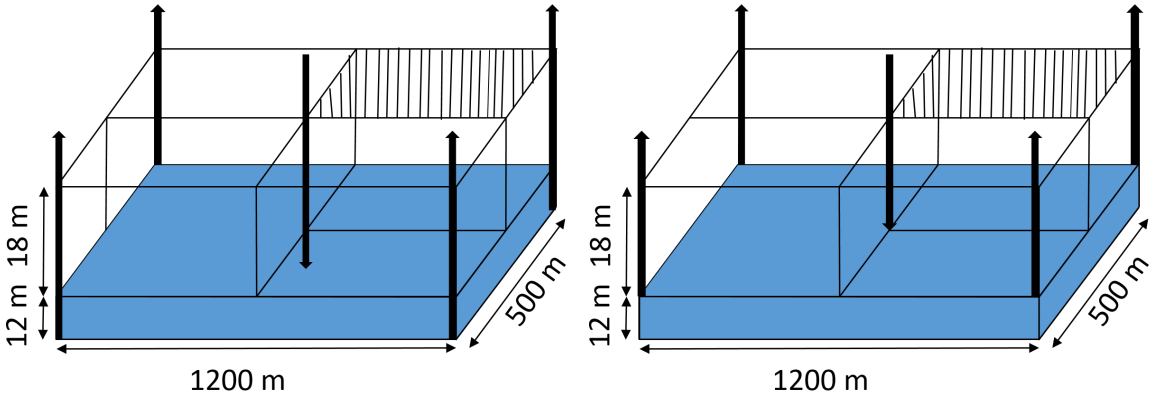

(a) Well placement in case-3

(b) Well placement in case-4

Figure 6: Well completed vertically in case-3 and case-4

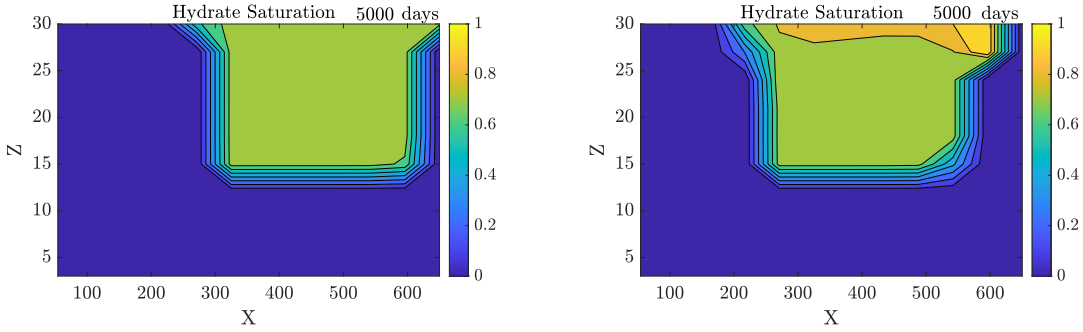

(a) Saturation of hydrate at 5000 days for case-3

(b) Saturation of hydrate at 5000 days for case-4

Figure 7: Profiles for hydrate saturation of 5-spot vertical well pattern

Fig.5a shows that the cumulative gas production is 22% of OGIP in 5000 days for case-3 as compared to 16% of OGIP production for case-4. Fig.7 shows the profiles for hydrate saturation at 5000 days for both the cases. X-axis is the diagonal connecting the injector at left to the producer at right and z-axis is the depth of the reservoir. The colour shows the hydrate saturation. From Fig.7 we gather that most of the hydrate dissociates near the injector. This is because, the depressurization is ineffective, and increase in reservoir temperature by warm water injection leads to hydrate dissociation. When wells are placed in the aquifer, the temperature increase near the bottom of the hydrate bearing zone is more, leading to more gas production in case-3. This is because of the higher water injectivity in the aquifer zone where the two wells are aligned which increase the horizontal convection of warm water. This also leads to the higher water production as shown by gas water ratio (GWR) in the Fig.5b. 22% of OGIP production is still less, therefore, we investigate the production using horizontal placement of the wells for warm water injection.

3.3. ***Thermal stimulation and depressurization using horizontal wells:***

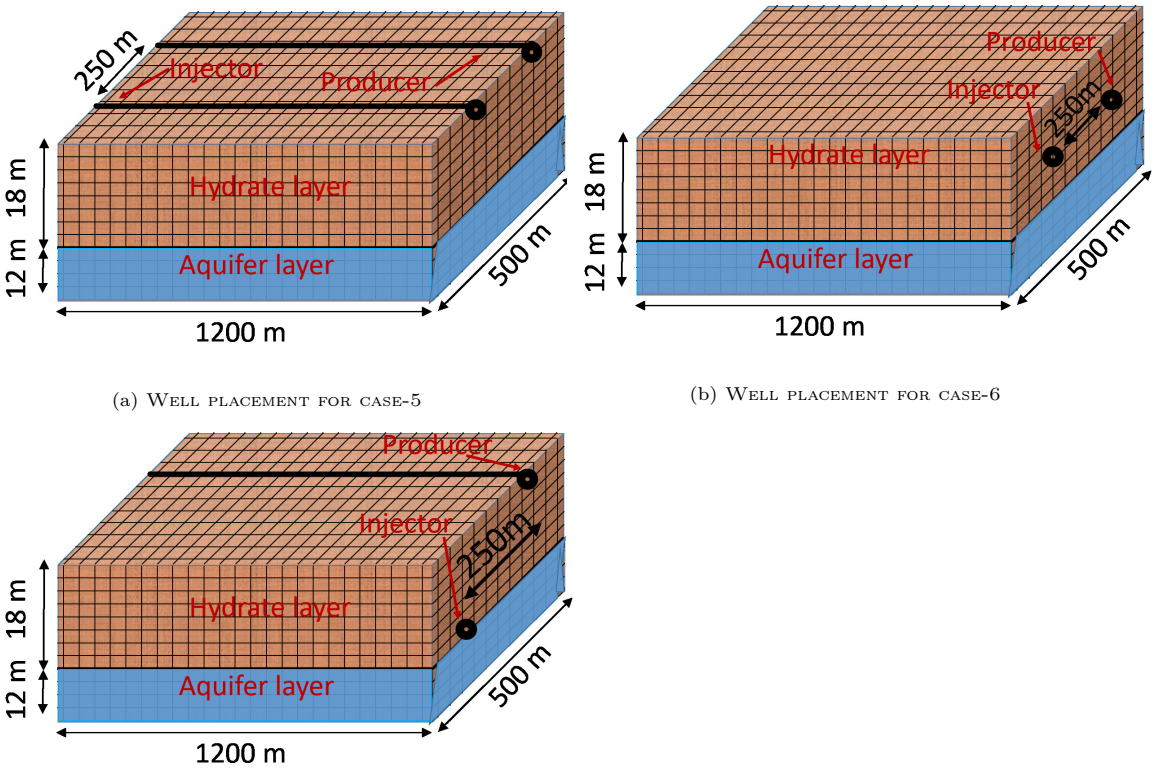

(a) Well placement for case-5

(b) Well placement for case-6

(c) Well placement for case-7

Figure 8: Wells completed horizontally in case-5, case-6 and case-7

We now consider horizontal well placement, where the injector and producer are located 250m apart from each other along the length of the reservoir, shown in Fig.8. Three different cases are considered, case-5, case-6 and case7, having horizontal placement of wells as shown in Table.3. Fig.8a shows case-5 where both the injector and the producer are placed horizontally at the top of hydrate zone. Fig.5a shows that the gas production is 47% of OGIP for this case. There is

insignificant production for the first 700 days, after which the production rate is higher. We see from the hydrate saturation profile in Fig.9a, showing a plane perpendicular to the wells that initially the warm water injection in the hydrate bearing layer is very slow because of the low permeability. However, when high permeability communication is established between the injection well and aquifer at around 700 days, the injected warm water dissociate hydrates near the aquifer, shown by hydrate saturation profile in Fig.9a. To complement our hypothesis of aquifer helping in hydrate dissociation, we consider case-6, where the injector and producer are horizontally placed in the middle of the hydrate bearing sediments, shown in Fig.8b. In this case also our simulations show the cumulative production of 47% of OGIP. Fig.9b shows hydrate saturation profiles and we see that the communication between injection well and aquifer is established at 500 days. In the production curve, in Fig.5a we see that the production is insignificant for about 500 days of the production operation and then increases. Therefore, if we want the production to start from the beginning, we need to have warm water injector near the aquifer. Fig.8c shows case-7, where injector is located near the aquifer and producer at the top of the hydrate zone. We see that cumulative gas production is 47% of OGIP and the production starts from the very beginning of the well operation which is shown in Fig.5a. Fig.9c confirms our hypothesis showing the profiles of hydrate saturation at 100 days, where the dissociation starts near the water layer from the first day of the production operation. Water production is higher in all the three cases as shown in Fig.5b. When the injector is located in the hydrate layer water production increases once the dissociation front hits the aquifer layer but in case-7 the water production is high from the very beginning.

3.4. ***Combination of vertical and horizontal wells for hydrate production:***

Further, to increase the productivity and improve the economics by having one vertical well, we consider two different cases of horizontal and vertical wells as described case-8 and case-9 in Table.3. In case-8, injector is placed horizontally at the top layer of the reservoir block and vertical producer completed in the hydrate and aquifer zone at the right side of the reservoir as shown in Fig.10a. In case-9, producer is placed horizontally at the top layer of the hydrate zone and injector placed vertically on the left side of the reservoir, as shown in Fig.10b. The total gas production in case-8 is ($47\% of OGIP$), same as the cases where both the wells are placed horizontally. The cumulative gas production in case-9 is (6%) in 5000 days, the smallest of all the cases where warm water is injected, as shown in Fig.5a. This is because the warm water injected vertically leaks out of the reservoir and goes to the aquifer below. Moreover, the horizontally placed producer at the top is unable to provide enough suction to the injected warm water because the wells are not aligned as in case-1 where the vertical wells are aligned and facilitate the horizontal convection of warm water near the aquifer leading 16% recovery of gas. The pressure near the injector does not decrease resulting in the less hydrate dissociation evident from hydrate saturation profile in Fig.11b for case-9. However, in case-8 most of the production is due to the warm water injection as we can see it in hydrate saturation profile in Fig.11a. The significant production of the gas in case-8 starts from 700 days similar to case-5.

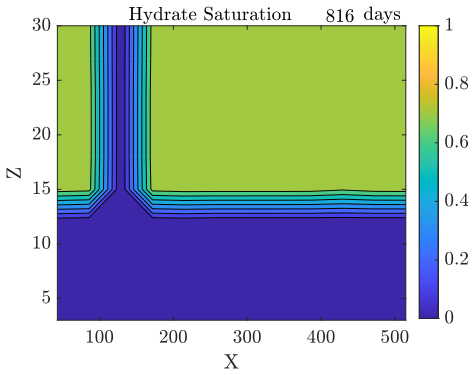

(a) Saturation of hydrate at 816 days for case-5

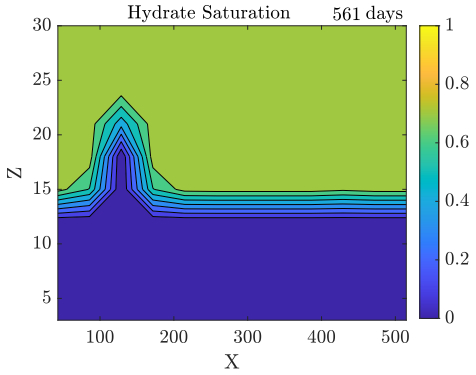

(b) Saturation of hydrate at 561 days for case-6

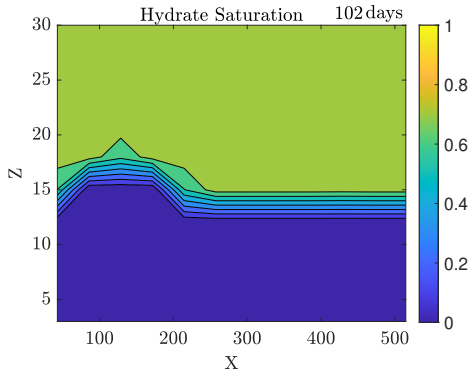

(c) Saturation of hydrate at 100 days for case-7

Figure 9: Profiles of hydrate saturation for case-5, case-6, case-7

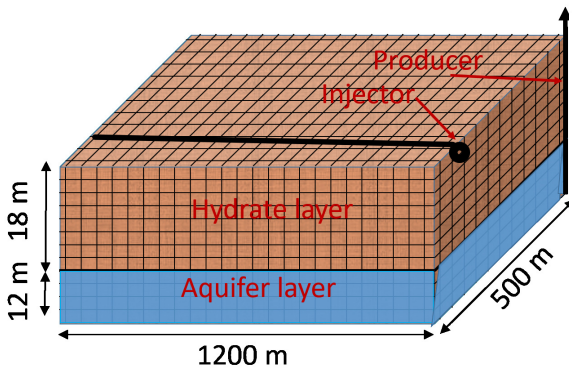

(a) Well placement for case-8

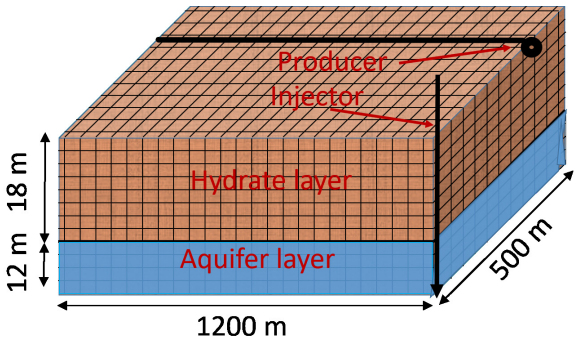

(b) Well placement for case-9

Figure 10: Well completion for case-8 and case-9

3.5. Sensitivity towards temperature and pressure

We find from the above analysis that warm water injection has a major impact on the gas production from gas hydrate reservoirs. If the initial reservoir pressure increases then we need to increase the injection pressure to inject sufficient amount of warm water. We now analyze the sensitivity of initial and injection pressure on methane production using case-7 above. We assume that the initial pressure can vary between 25 MPa to 35 MPa as it is evident in Fig.2. In the previous simulations we assumed the initial pressure is 31 MPa as shown in Fig.3. If all

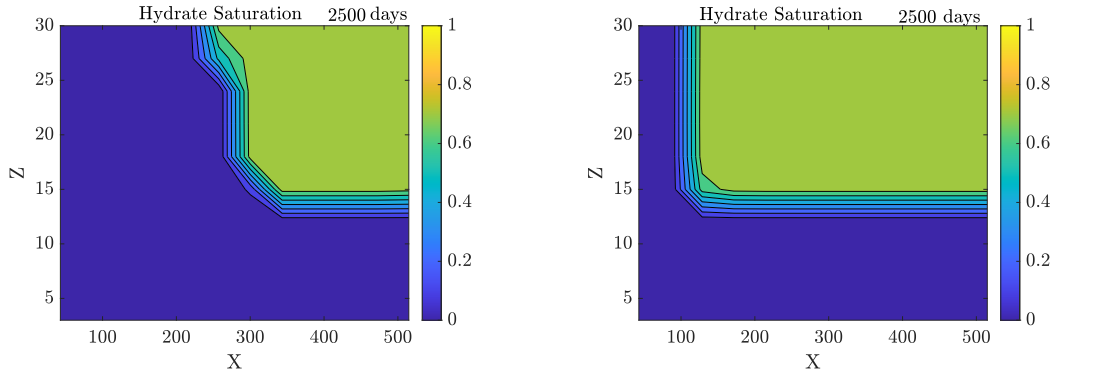

(a) Saturation of hydrate at 2500 days for case-8

(b) Saturation of hydrate at 2500 days for case-9

Figure 11: Profiles for hydrate saturation of case-8 and case-9

other conditions of the reservoir and the operating conditions of the injector and the producer are same, then Fig.12a shows the gas production curves at different initial pressures. The highest gas production is observed in case when initial reservoir pressure is 25 MPa as shown in Fig.12a. In this case, the depressurization at production well becomes effective as the initial pressure is low. There is sudden increase in the gas production once the dissociation front due to depressurization reaches the aquifer layer at 2600 days as shown in Fig.13. This is because the injected warm water provides the heat of dissociation and when the dissociation fronts originating at the injector meets the dissociation front originating at the producer, the warm water convection increases. This increases the dissociation of hydrate leading to higher gas production as seen in Fig.13. The cumulative gas production is more than 80 % of OGIP at 25 MPa initial reservoir pressure. At higher initial reservoir pressure, the water injection is low and the pressure reduction at the production well is ineffective. Therefore, the cumulative gas production at the higher initial pressure of the reservoir is less than 50% of OGIP as shown in Fig.12a. We see that, in order to enhance the gas production from the reservoir at higher initial pressure, the injection pressure or injection temperature has to be increased. Next, we study the impact of injection pressure on the gas production at different initial pressure where the injection temperature is 323.2 K same as all the other cases shown in Fig.12b. In Fig.12b, the red colour is used to represent all the different cases of injection pressure (InjP) where initial pressure (IP) is 25 MPa(IP-25), blue colour is used for IP-29, black for IP-31 and magenta for IP-35. From Fig.12b it is evident that the injection pressure alone does not have much impact on the gas production.

Further we analyzed the sensitivity of gas production for the producer well pressure from 3 MPa to 4.5 MPa and injection water temperature from 320K to 330K and did not observe any significant difference. Thermodynamically the variation is significant to release methane at higher temperature or lower pressure. However, in this work, we have considered unconfined gas hydrate reservoirs which has an infinite aquifer layer present below the hydrate layer that does not allow the decrease in the pressure to impact the dissociation around the production well. Therefore, the pressure at the producer well does not have significant impact on the total production [19, 74]. The temperature variation is also thermodynamically significant, however, in our reservoir model

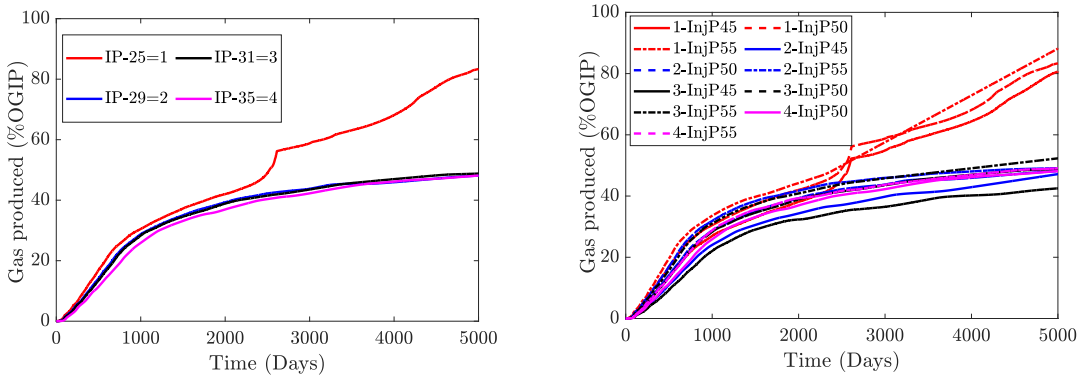

(a) Gas production at different initial pressure in % OGIP

(b) Gas produced at different injection pressure in % OGIP

Figure 12: Impact of initial pressure of the reservoir and well injection pressure on the gas production

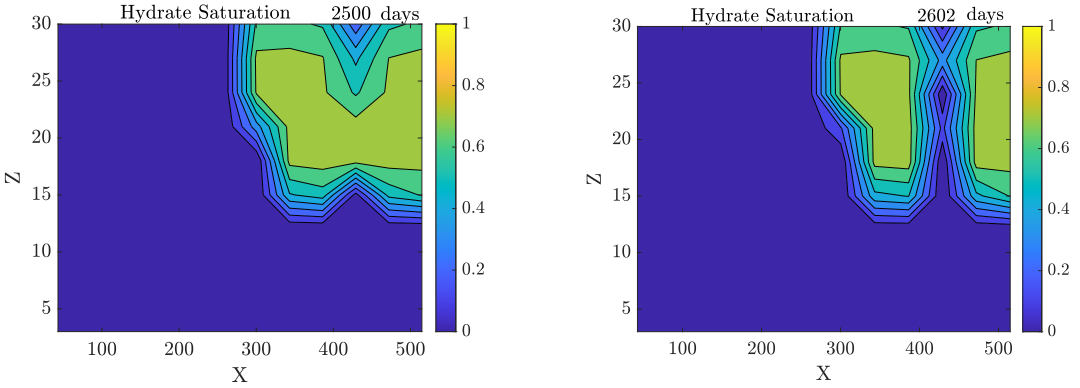

(a) Saturation profile for $IP-25$ at 2500 days

(b) Saturation profile for $IP-25$ at 2600 days

Figure 13: Saturation profiles for $IP-25$

the infinite aquifer acts as a sink for the injected water, that control the overall gas production.

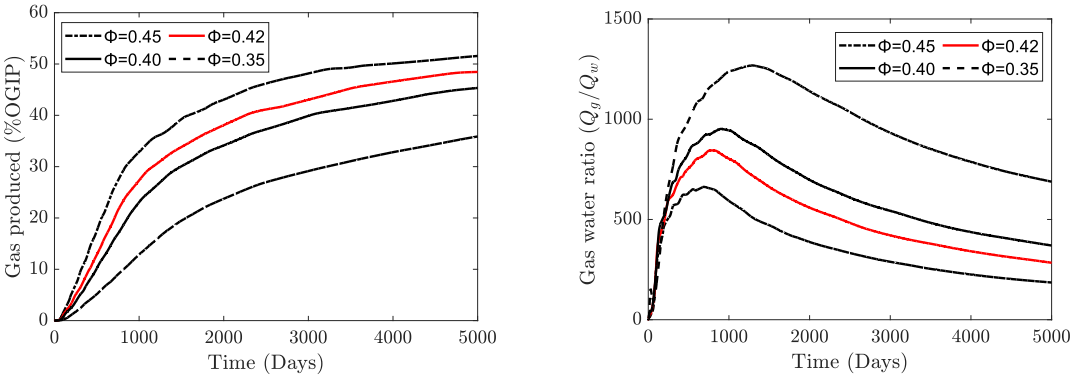

(a) Gas production for homogeneous reservoir cases at different porosity in % OGIP

(b) Gas water ratio for homogeneous reservoir cases at different porosity

Figure 14: Gas production profiles (in % OGIP) and Gas water ratio for homogeneous reservoir cases at different porosity

3.6. ***Sensitivity of gas recovery towards porosity***

We perform sensitivity analysis for porosity of the reservoir. We have used Civan's Power law model in our simulations which correlates porosity and permeability as given in equation 5. The presence of hydrate also changes the effective porosity and hence permeability [64, 75]. Fig.14a shows the gas recovery from the reservoir at different initial reservoir porosity when initial hydrate saturation is 0.75, same as all previous cases. It is evident from Fig.14a that when the reservoir porosity is low the percentage gas recovery is also low. The gas water ratio also decreases with porosity as shown in Fig.14b. This means that the fraction of water being produced also decreases with decrease in porosity. There are competing forces when the porosity is decreased- 1) The total energy available for the dissociation of hydrate is more due to more sediments at lower porosity value, which can provide sensible heat during dissociation. 2) However, low porosity and hence low permeability limits the water injection which reduces the heat injection to the reservoir and leads to the decreased gas and water production. Due to decrease in the warm water injection at low porosity we observe decrease in hydrate dissociation leading to less gas production (Fig.14a) and less water production from the reservoir leading to more gas water ratio (Fig.14b)

3.7. ***Sensitivity towards reservoir heterogeneity***

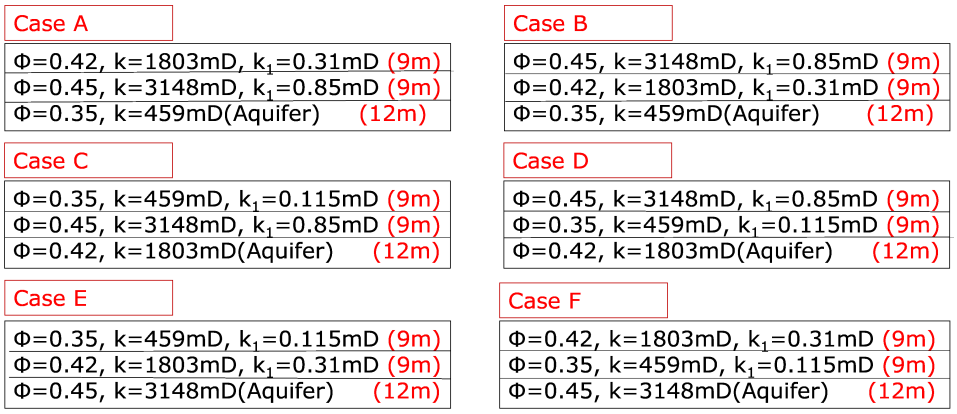

Figure 15: Description of heterogeneous reservoir model

In the above analysis, we considered homogeneous reservoir block where the initial permeability is constant for the entire reservoir block. However, the gas hydrate reservoirs in the nature are heterogeneous predominantly due to geological layering of the sediments [17, 61, 62]. In the present work, we analyze the sensitivity of gas production using horizontal wells for the reservoir heterogeneity. We use well placement same as in the case-7 above in section 3.3. Six different heterogeneous reservoir cases are considered, where different porosity is considered for the layers as shown in Fig.15. The permeability of the hydrate free sand (k) and the sand having 0.75 saturation of hydrate (k_1) for the porosity which is considered in the layered reservoir are given in Fig.15. The final gas production and the gas water ratio for all the different cases is shown in Fig.16.

We compared the cases where the infinite aquifer layer has the same effective permeability. In Fig.16a, case A and case B, have similar permeability of the aquifer layer. The overall gas

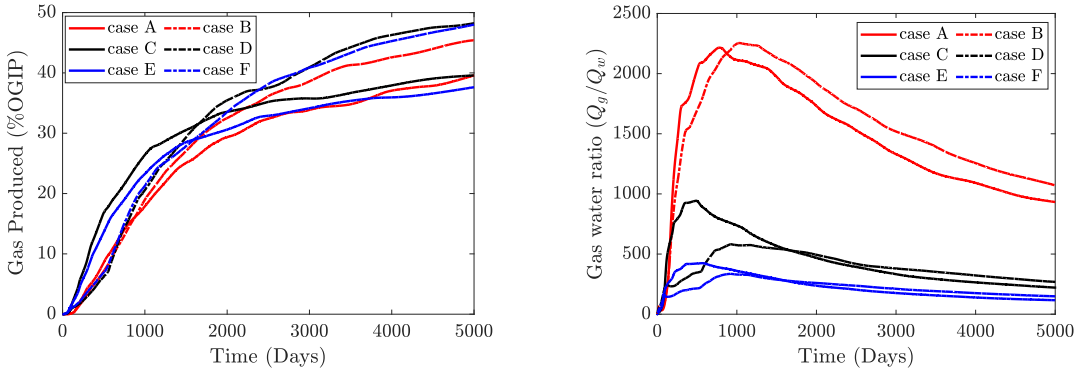

(a) Gas production for heterogeneous reservoir cases at different porosity in % OGIP

(b) Gas water ratio for heterogeneous reservoir cases at different porosity

Figure 16: Gas production profiles (in % OGIP) and Gas water ratio for heterogeneous reservoir cases at different porosity

recovery is higher in case B where permeability is higher at the top layer of the hydrate zone as compared to the case A. Similarly, when we compare case C and case D having the same aquifer permeability, the gas production is higher in case D when the permeability of the top layer is more. The similar pattern can also be observed in case E and case F. This observation suggests that when the permeability of the top hydrate layer is more, the availability of the enthalpy of the dissociation from overburden leads to more gas production regardless of the variation in the bottom hydrate layer.

From Fig.16b, we observe from gas water ratio (GWR) that the aquifer layer has more impact on the water production in comparison to the gas production. When the permeability of the aquifer is less, water production reduced as we compare GWR for case C and case D with GWR of case A and case B. The results suggests that in an unconfined layered gas hydrate reservoir where we use thermal stimulation as well as the depressurization method, gas production is affected by the topmost layer of the hydrate bearing zone the most and water production is more sensitive towards the aquifer permeability.

4. Conclusion

Warm water injection is crucial for methane gas production from unconfined class-2 gas hydrate reservoirs as depressurization is ineffective. Horizontal injector configuration in marine, high pressure hydrate reservoir are more productive than vertical injectors. However, the horizontal producer does not have notable impact on the gas production. From the work above, we observe that the proximity of the horizontal injector with unconfined aquifer leads to the early gas production while the overall gas production remains the same. This is due to the permeability of the aquifer zone which helps in convection of the warm water near the hydrate-water contact line. We also observe that if the initial pressure of the reservoir is less, then the depressurization also becomes effective and overall gas recovery is approx 80% of OGIP. The producer well pressure and the injection water temperature does not have significant effect on the gas production as long as

the water temperature is high enough for dissociation. The gas production is sensitive towards the porosity in the reservoir as it governs the warm water injection rate and injection volume, thus governing the dissociation energy available to gas hydrates. Therefore, low porosity reservoirs will have low recovery factors. In a layered reservoir, it is interesting to note that the permeability of layer near the overburden significantly affect the gas production due to accessibility of the dissociation energy from the overburden. The infinite aquifer layer has impact on the water production, but the overall gas production is not significantly affected by the aquifer alone. On the whole, the well placement and the well configuration play a significant role along with the effective permeability of the different layers in gas production from the gas hydrate reservoir. The optimal production strategy explored in this study can be helpful in investigating the long-term production potential of the class-2 unconfined reservoirs. The sensitivity analysis results can be incorporated to understand the geological complexities of the reservoirs and to enhance the accuracy of gas production potential of reservoirs through simulation.

Acknowledgment

The authors thank Science and Engineering Board (SERB), India (Diary No. SERB/ F/1297/2017-18, File No. ECR/2017/000257) for the financial support.

References

References

[1] M. T. Reagan, G. J. Moridis, J. N. Johnson, L. Pan, C. M. Freeman, K. L. Boyle, N. D. Keen, J. Husebo, Field-scale simulation of production from oceanic gas hydrate deposits, Transport in Porous Media 108 (1) (2015) 151–169.

[2] K. A. Kvenvolden, Gas hydrates—geological perspective and global change, Reviews of geophysics 31 (2) (1993) 173–187.

[3] G. Bhatnagar, W. G. Chapman, G. R. Dickens, B. Dugan, G. J. Hirasaki, Scaling of thermodynamic and transport processes for predicting methane hydrate saturation in marine sediments worldwide, in: SPE Annual Technical Conference and Exhibition, OnePetro, 2006.

[4] K. A. Kvenvolden, Potential effects of gas hydrate on human welfare, Proceedings of the National Academy of Sciences 96 (7) (1999) 3420–3426.

[5] R. Matsumoto, Comparison of marine and permafrost gas hydrates: Examples from nankai trough and mackenzie delta, Proc. 4th ICGH, 2002 (2002) 1–6.

[6] S. P. Hesselbo, D. R. Gröcke, H. C. Jenkyns, C. J. Bjerrum, P. Farrimond, H. S. M. Bell, O. R. Green, Massive dissociation of gas hydrate during a jurassic oceanic anoxic event, Nature 406 (6794) (2000) 392.

[7] E. Brook, D. Archer, S. Frolking, D. Lawrence, Potential for abrupt changes in atmospheric methane (2008).

[8] V. Krey, J. G. Canadell, N. Nakicenovic, Y. Abe, H. Andruleit, D. Archer, A. Grubler, N. T. Hamilton, A. Johnson, V. Kostov, et al., Gas hydrates: entrance to a methane age or climate threat?, Environmental Research Letters 4 (3) (2009) 034007.

[9] P. U. Clark, A. J. Weaver, E. J. Brook, K. Steffen, E. R. Cook, T. L. Delworth, Abrupt Climate Change: Report, Vol. 3, US Climate Change Science Program, 2008.

[10] D. Archer, Methane hydrate stability and anthropogenic climate change, Biogeosciences 4 (4) (2007) 521–544.

[11] E. D. Sloan Jr, Clathrate Hydrates of Natural Gases, revised and expanded, CRC press, 1998.

[12] P. Bhade, J. Phirani, Gas production from layered methane hydrate reservoirs, Energy 82 (2015) 686–696.

[13] Y. Cheng, L. Li, Z. Yuan, L. Wu, S. Mahmood, Finite element simulation for fluid–solid coupling effect on depressurization-induced gas production from gas hydrate reservoirs, Journal of Natural Gas Science and Engineering 10 (2013) 1–7.

[14] G. Li, B. Li, X.-S. Li, Y. Zhang, Y. Wang, Experimental and numerical studies on gas production from methane hydrate in porous media by depressurization in pilot-scale hydrate simulator, Energy & Fuels 26 (10) (2012) 6300–6310.

[15] M. Uddin, F. Wright, S. Dallimore, D. Coombe, Gas hydrate dissociations in mallik hydrate bearing zones a, b, and c by depressurization: Effect of salinity and hydration number in hydrate dissociation, Journal of Natural Gas Science and Engineering 21 (2014) 40–63.

[16] Y. Makogon, R. Omelchenko, Commercial gas production from messoyakha deposit in hydrate conditions, Journal of Natural Gas Science and Engineering 11 (2013) 1–6.

[17] P. Bhade, J. Phirani, Effect of geological layers on hydrate dissociation in natural gas hydrate reservoirs, Journal of Natural Gas Science and Engineering 26 (2015) 1549–1560.

[18] J. Phirani, K. Mohanty, Warm water flooding of confined gas hydrate reservoirs, Chemical Engineering Science 64 (10) (2009) 2361–2369.

[19] J. Phirani, K. K. Mohanty, G. J. Hirasaki, Warm water flooding of unconfined gas hydrate reservoirs, Energy & Fuels 23 (9) (2009) 4507–4514.

[20] M. J. Castaldi, Y. Zhou, T. M. Yegulalp, Down-hole combustion method for gas production from methane hydrates, Journal of petroleum Science and Engineering 56 (1-3) (2007) 176–185.

[21] V. A. Kamath, S. P. Godbole, et al., Evaluation of hot-brine stimulation technique for gas production from natural gas hydrates, Journal of petroleum technology 39 (11) (1987) 1–379.

[22] J. Phirani, K. K. Mohanty, G. J. Hirasaki, Warm water flooding of unconfined gas hydrate reservoirs, Energy & Fuels 23 (9) (2009) 4507–4514.

[23] F. Dong, X. Zang, D. Li, S. Fan, D. Liang, Experimental investigation on propane hydrate dissociation by high concentration methanol and ethylene glycol solution injection, Energy & Fuels 23 (3) (2009) 1563–1567.

[24] G. Li, X.-S. Li, L.-G. Tang, Y. Zhang, Experimental investigation of production behavior of methane hydrate under ethylene glycol injection in unconsolidated sediment, Energy & fuels 21 (6) (2007) 3388–3393.

[25] J. Sira, S. Patil, V. Kamath, et al., Study of hydrate dissociation by methanol and glycol injection, in: SPE Annual technical conference and exhibition, Society of Petroleum Engineers, 1990.

[26] I. F. Makogon, I. F. Makogon, Y. F. Makogon, Hydrates of hydrocarbons, Pennwell Books, 1997.

[27] J. Lee, Experimental study on the dissociation behavior and productivity of gas hydrate by brine injection scheme in porous rock, Energy & Fuels 24 (1) (2009) 456–463.

[28] A. Graue, B. Kvamme, B. A. Baldwin, J. Stevens, J. J. Howard, G. Ersland, J. Husebo, D. R. Zornes, et al., Magnetic resonance imaging of methane-carbon dioxide hydrate reactions in sandstone pores, in: SPE Annual Technical Conference and Exhibition, Society of Petroleum Engineers, 2006.

[29] V. Mohebbi, R. Behbahani, Experimental study on gas hydrate formation from natural gas mixture, Journal of Natural Gas Science and Engineering 18 (2014) 47–52.

[30] J. Phirani, K. K. Mohanty, et al., Kinetic simulation of co2 flooding of methane hydrates, in: SPE Annual Technical Conference and Exhibition, Society of Petroleum Engineers, 2010.

[31] Y. Park, D.-Y. Kim, J.-W. Lee, D.-G. Huh, K.-P. Park, J. Lee, H. Lee, Sequestering carbon dioxide into complex structures of naturally occurring gas hydrates, Proceedings of the National Academy of Sciences 103 (34) (2006) 12690–12694.

[32] A. Nago, A. Nieto, Natural gas production from methane hydrate deposits using co 2 clathrate sequestration: State-of-the-art review and new technical approaches., Journal of Geological Research 2011 (2011).

[33] K. Ohgaki, K. Takano, H. Sangawa, T. Matsubara, S. Nakano, Methane exploitation by carbon dioxide from gas hydrates—phase equilibria for co2-ch4 mixed hydrate system—, Journal of chemical engineering of Japan 29 (3) (1996) 478–483.

[34] N. Goel, In situ methane hydrate dissociation with carbon dioxide sequestration: Current knowledge and issues, Journal of petroleum science and engineering 51 (3-4) (2006) 169–184.

[35] J. Zhao, Y. Liu, X. Guo, R. Wei, T. Yu, L. Xu, L. Sun, L. Yang, Gas production behavior from hydrate-bearing fine natural sediments through optimized step-wise depressurization, Applied Energy 260 (2020) 114275.

[36] T. S. Collett, R. Boswell, J. R. Cochran, P. Kumar, M. Lall, A. Mazumdar, M. V. Ramana, T. Ramprasad, M. Riedel, K. Sain, et al., Geologic implications of gas hydrates in the offshore of india: Results of the national gas hydrate program expedition 01, Marine and Petroleum Geology 58 (2014) 3–28.

[37] Y. F. Makogon, Natural gas hydrates–a promising source of energy, Journal of Natural Gas Science and Engineering 2 (1) (2010) 49–59.

[38] A. V. Milkov, R. Sassen, Estimate of gas hydrate resource, northwestern gulf of mexico continental slope, Marine Geology 179 (1-2) (2001) 71–83.

[39] R. Boswell, D. Shelander, M. Lee, T. Latham, T. Collett, G. Guerin, G. Moridis, M. Reagan, D. Goldberg, Occurrence of gas hydrate in oligocene frio sand: Alaminos canyon block 818: Northern gulf of mexico, Marine and Petroleum Geology 26 (8) (2009) 1499–1512.

[40] G. J. Moridis, M. T. Reagan, A. F. Queiruga, R. Boswell, Evaluation of the performance of the oceanic hydrate accumulation at site nghp-02-09 in the krishna-godavari basin during a production test and during single and multi-well production scenarios, Marine and Petroleum Geology (2018).

[41] Y. ZHU, Y. ZHANG, H. WEN, Z. LU, Z. JIA, Y. LI, Q. LI, C. LIU, P. WANG, X. GUO, Gas hydrates in the qilian mountain permafrost, qinghai, northwest china, Acta Geologica Sinica-English Edition 84 (1) (2010) 1–10.

[42] S. Li, S. Li, R. Zheng, Q. Li, W. Pang, Strategies for gas production from class 2 hydrate accumulations by depressurization, Fuel 286 (2021) 119380.

[43] Y. Wang, X.-S. Li, G. Li, Y. Zhang, B. Li, J.-C. Feng, A three-dimensional study on methane hydrate decomposition with different methods using five-spot well, Applied energy 112 (2013) 83–92.

[44] J. Zhao, Z. Fan, B. Wang, H. Dong, Y. Liu, Y. Song, Simulation of microwave stimulation for the production of gas from methane hydrate sediment, Applied Energy 168 (2016) 25–37.

[45] B. Wang, H. Dong, Z. Fan, S. Liu, X. Lv, Q. Li, J. Zhao, Numerical analysis of microwave stimulation for enhancing energy recovery from depressurized methane hydrate sediments, Applied Energy 262 (2020) 114559.

[46] R. Boswell, E. Myshakin, G. Moridis, Y. Konno, T. S. Collett, M. Reagan, T. Ajayi, Y. Seol, India national gas hydrate program expedition 02 summary of scientific results: Numerical simulation of reservoir response to depressurization, Marine and Petroleum Geology (2018).

[47] K. Yamamoto, T. Kanno, X.-X. Wang, M. Tamaki, T. Fujii, S.-S. Chee, X.-W. Wang, V. Pimenov, V. Shako, Thermal responses of a gas hydrate-bearing sediment to a depressurization operation, Rsc Advances 7 (10) (2017) 5554–5577.

[48] Agency for Natural Resources and Energy (ANRE) and Japan Oil, Gas and Metals National Corporation (JOGMEC), "second offshore methane hydrate production test finishes", https://www.meti.go.jp/english/press/2017/0629_001.html, accessed: 2017-06-29 (2017).

[49] Z. Hao, H. Fei, Q. Hao, L. Liu, China has successfully conducted its first pilot production of natural gas hydrates, Acta Geol. Sin. 91 (3) (2017) 1133–1134.

[50] E. M. Myshakin, M. Gaddipati, K. Rose, B. J. Anderson, Numerical simulations of depressurization-induced gas production from gas hydrate reservoirs at the walker ridge 313 site, northern gulf of mexico, Marine and petroleum geology 34 (1) (2012) 169–185.

[51] E. M. Myshakin, Y. Seol, J.-S. Lin, S. Uchida, T. S. Collett, R. Boswell, Numerical simulations of depressurization-induced gas production from an interbedded turbidite gas hydrate-bearing sedimentary section in the offshore india: Site nghp-02-16 (area-b), Marine and Petroleum Geology (2018).

[52] M. Kurihara, H. Ouchi, H. Narita, Y. Masuda, Gas production from methane hydrate reservoirs, in: Proceedings of the 7th International Conference on Gas Hydrates (ICGH 2011), Edinburgh, Scotland, United Kingdom, 2011.

[53] G. Moridis, et al., Numerical studies of gas production from class 2 and class 3 hydrate accumulations at the mallik site, mackenzie delta, canada, SPE Reservoir Evaluation & Engineering 7 (03) (2004) 175–183.

[54] Ş. Merey, Drilling of gas hydrate reservoirs, Journal of Natural Gas Science and Engineering 35 (2016) 1167–1179.

[55] Ş. Merey, S. N. Longinos, Numerical simulations of gas production from class 1 hydrate and class 3 hydrate in the nile delta of the mediterranean sea, Journal of Natural Gas Science and Engineering 52 (2018) 248–266.

[56] G. J. Moridis, E. D. Sloan, Gas production potential of disperse low-saturation hydrate accumulations in oceanic sediments, Energy conversion and management 48 (6) (2007) 1834–1849.

[57] G. J. Moridis, Toward production from gas hydrates: current status, assessment of resources, and simulation-based evaluation of technology and potential (2008).

[58] J. Sun, F. Ning, L. Zhang, T. Liu, L. Peng, Z. Liu, C. Li, G. Jiang, Numerical simulation on gas production from hydrate reservoir at the 1st offshore test site in the eastern nankai trough, Journal of Natural Gas Science and Engineering 30 (2016) 64–76.

[59] Y. Konno, A. Kato, J. Yoneda, M. Oshima, M. Kida, Y. Jin, J. Nagao, N. Tenma, Numerical analysis of gas production potential from a gas-hydrate reservoir at site nghp-02-16, the krishna–godavari basin, offshore india–feasibility of depressurization method for ultra-deepwater environment, Marine and Petroleum Geology (2018).

[60] J. Zhao, T. Yu, Y. Song, D. Liu, W. Liu, Y. Liu, M. Yang, X. Ruan, Y. Li, Numerical simulation of gas production from hydrate deposits using a single vertical well by depressurization in the qilian mountain permafrost, qinghai-tibet plateau, china, Energy 52 (2013) 308–319.

[61] S. Jana, M. Ojha, K. Sain, S. Srivastava, An approach to estimate gas hydrate saturation from 3-d heterogeneous resistivity model: A study from krishna-godavari basin, eastern indian offshore, Marine and Petroleum Geology 79 (2017) 99–107.

[62] M. Tamaki, T. Fujii, K. Suzuki, Characterization and prediction of the gas hydrate reservoir at the second offshore gas production test site in the eastern nankai trough, japan, Energies 10 (10) (2017) 1678.

[63] G. J. Moridis, M. Reagan, A. Queiruga, Analysis of the flow, thermal and geomechanical behavior of offshore hydrate deposits at the nghp-02-09-a site during short-and long-term gas production scenarios, in: AGU Fall Meeting Abstracts, 2017.

[64] X. Qin, Q. Liang, J. Ye, L. Yang, H. Qiu, W. Xie, J. Liang, C. Lu, H. Lu, B. Ma, et al., The response of temperature and pressure of hydrate reservoirs in the first gas hydrate production test in south china sea, Applied Energy 278 (2020) 115649.

[65] X. Sun, K. K. Mohanty, Kinetic simulation of methane hydrate formation and dissociation in porous media, Chemical Engineering Science 61 (11) (2006) 3476–3495.

[66] H. Kim, P. R. Bishnoi, R. A. Heidemann, S. S. Rizvi, Kinetics of methane hydrate decomposition, Chemical engineering science 42 (7) (1987) 1645–1653.

[67] R. W. Falta, K. Pruess, I. Javandel, P. A. Witherspoon, Numerical modeling of steam injection for the removal of nonaqueous phase liquids from the subsurface: 1. numerical formulation, Water Resources Research 28 (2) (1992) 433–449.

[68] J. W. Wilder, G. J. Moridis, S. J. Wilson, M. Kurihara, M. D. White, Y. Masuda, B. J. Anderson, T. S. Collett, R. B. Hunter, H. Narita, et al., An international effort to compare gas hydrate reservoir simulators, in: Proceedings of 6th International Conference on Gas Hydrates (ICGH 2008), Vancouver, CANADA, 2008.

[69] J. Phirani, R. Pitchumani, K. K. Mohanty, et al., History matching of hydrate formation and dissociation experiments in porous media, in: SPE Reservoir Simulation Symposium, Society of Petroleum Engineers, 2009.

[70] F. Civan, Scale effect on porosity and permeability: Kinetics, model, and correlation, AIChE journal 47 (2) (2001) 271–287.

[71] F. Civan, et al., Relating permeability to pore connectivity using a power-law flow unit equation, Petrophysics 43 (06) (2002).

[72] F. Civan, et al., Fractal formulation of the porosity and permeability relationship resulting in a power-law flow units equation-a leaky-tube model, in: International Symposium and Exhibition on Formation Damage Control, Society of Petroleum Engineers, 2002.

[73] R. Brooks, T. Corey, Hydrau uc properties of porous media, Hydrology Papers, Colorado State University 24 (1964) 37.

[74] G. Jin, T. Xu, X. Xin, M. Wei, C. Liu, Numerical evaluation of the methane production from unconfined gas hydrate-bearing sediment by thermal stimulation and depressurization in shenhu area, south china sea, Journal of Natural Gas Science and Engineering 33 (2016) 497–508.

[75] X. Sun, T. Luo, L. Wang, H. Wang, Y. Song, Y. Li, Numerical simulation of gas recovery from a low-permeability hydrate reservoir by depressurization, Applied energy 250 (2019) 7–18.